Surface & Coatings Technology 236 (2013) 320–325

Contents lists available at ScienceDirect

Surface & Coatings Technology

journal homepage: www.elsevier.com/locate/surfcoat

Graded nanostructured interfacial layers fabricated by high power pulsed magnetron sputtering — plasma immersion ion implantation and deposition (HPPMS–PIII&D)

Zhongzhen Wu [a,b], Xiubo Tian [a,*], Yongqiang Wei [a], Chunzhi Gong [a], Shiqin Yang [a], Feng Pan [b,**], Paul K. Chu [c]

[a] State Key Laboratory of Advanced Welding and Joining, Harbin Institute of Technology, Harbin 150001, China
[b] School of Advanced Materials, Shenzhen Graduate School, Peking University, Shenzhen 518055, China
[c] Department of Physics and Materials Science, City University of Hong Kong, Tat Chee Avenue, Kowloon, Hong Kong, China

ARTICLE INFO

Article history:
Received 11 July 2013
Accepted in revised form 8 October 2013
Available online 16 October 2013

Keywords:
High-power pulsed magnetron sputtering
Plasma immersion ion implantation and deposition
CrN layer
Stress
Interface

ABSTRACT

A nanostructured interfacial layer with a graded structure is produced by hybrid high-power pulsed magnetron sputtering–plasma immersion ion implantation and deposition (HPPMS–PIII&D) to improve adhesion of multi-functional coatings. As a demonstration, a ceramic CrN film is prepared on stainless steel together with a Cr interlayer. High-resolution transmission electron microscopy (HR-TEM) reveals the presence of a 40 nm thick nanostructured interfacial layer between the Cr interlayer and substrate with gradually changing compositions, and this layer which possesses a dense and pore/void free structure is responsible for the strong film adhesion. The hybrid technology combines the benefits of both the HPPMS and PIII&D enabling fabrication of functional films with the desired properties. The technique and fabrication strategy have many potential applications in photovoltaics, energy storage, tribology, lubrication, aeronautics, and astronautics.

© 2013 Published by Elsevier B.V.

1. Introduction

Thin films are widely used in the fields of photovoltaics [1], energy storage [2], mechanics [3], lubrication [4], aeronautics, and astronautics [5] and film properties such as adhesion strength and stability depend on not only the film composition but also the interfacial structure between the film and substrate. The key to avoid failures such as delamination is minimization of the stress caused by the lattice and thermal mismatch among the various deposited layers and with the substrate [6]. The stress is especially severe in systems consisting of different types of materials such as ceramics and metals. Furthermore, different thermal expansion coefficients can lead to buckling, spallation, fracture, and surface roughening [7,8]. One of the means to relax the stress is to create an interfacial layer between the functional layer and substrate. As illustrated in Fig. 1, creation of interlayers I and II between the middle layer and top film/substrate, respectively, creates a structure with graded compositions to minimize the stress and enhance adhesion [9]. In most cases, interfacial layer I between the top and middle layer can be produced relatively easily by adjusting the deposition parameters, but it is more difficult to prepare a suitable layer II in Fig. 1 (d) to create a gradual compositional transition between the middle layer and substrate due to the typically big lattice mismatch and weak van der Waals forces [10]. Consequently, it is important to contrive the proper strategy to create the interfacial layers.

Plasma immersion ion implantation and deposition (PIII&D) can minimize interfacial stress and improve adhesion strength by introducing metallic ions energetically into the substrate to create ionic and covalent bonds [11,12]. However, the use of a unfiltered pulsed cathodic vacuum arc (PCVA) [13,14] produces liquid metal droplets with sizes of 100–1000 nm, usually referred to as macro-particles, that can adversely affect film deposition and properties [15,16]. Additionally, the interlayer II is typically quite thin (on the order of 10 nm) which is insufficient to relax the stress at the interface between the middle layer and substrate.

High-power pulsed magnetron sputtering (HPPMS) has been shown to produce large ion fluxes similar to an arc discharge [17,18], but does not suffer from macro-particle contamination. In this work, a hybrid technique combining HPPMS and PIII&D is introduced [19,20]. In this technique, HPPMS is used to produce the metal plasma to conduct PIII&D. To demonstrate the concept and practicality, a coating structure comprising a ceramic CrN film (top layer) and Cr film (middle layer) on stainless steel (substrate) is produced and the properties are investigated systematically. Our results show that the stress can be relaxed effectively by the nanostructured interface created by HPPMS–PIII&D.

2. Experimental section

The experiments were performed in a vacuum chamber with a diameter of 40 cm and height of 80 cm. The base pressure was 3×10^{-3} Pa and 99.9997% pure Ar (carrier gas) and 99.998% pure N_2 (reactive gas) were introduced. A Cr target (50 mm in diameter, 6 mm thick, and 99.9% pure) was mounted on an unbalanced magnetron cathode driven by a custom hybrid pulsed power supply to conduct

* Corresponding author. Tel./fax: 86 451 86418784.
** Corresponding author. Tel./fax: 86 755 26033200.
E-mail addresses: xiubotian@163.com (X. Tian), panfeng@pkusz.edu.cn (F. Pan).

0257-8972/$ – see front matter © 2013 Published by Elsevier B.V.
http://dx.doi.org/10.1016/j.surfcoat.2013.10.007

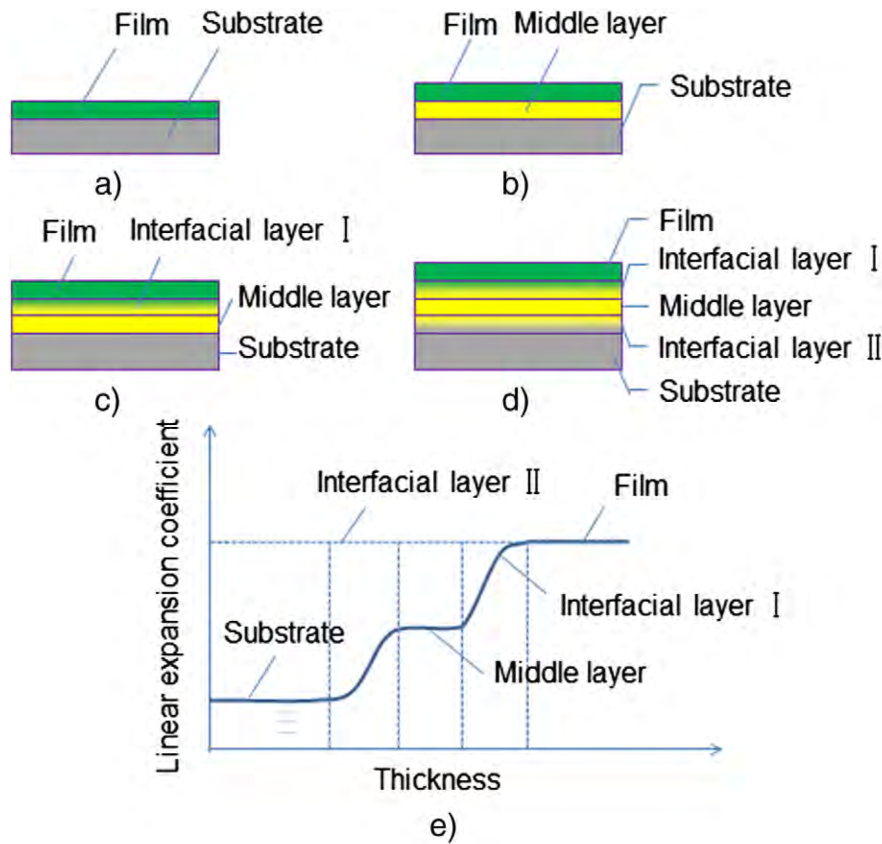

Fig. 1. Schematic diagram illustrating the interfacial design between the films and substrates, a) without interlayer, b) with middle layer, c) with middle layer and interfacial layer I and d) with middle layer, interfacial layer I and interfacial layer II, e) evolution of linear expansion coefficient in the interlayers between the films and substrates.

pretreatment and deposition. The substrate was biased by a pulsed high-voltage modulator delivering pulses of up to 30 kV (peak voltage) at 20–200 Hz with pulse widths between 20 and 500 μs. Silicon (100) and SU201 stainless steel samples (30 mm long, 30 mm wide, and 3 mm thick) were used as the substrates. The stainless steel samples were polished using 1 μm diamond paste. Prior to deposition, the substrates were ultrasonically cleaned in ethanol and acetone for 20 min. The substrates were placed at a distance of 16 cm from the target and no heating was applied.

Deposition was performed in three stages. First, the Cr layer was prepared on the SU201 stainless steel and Si (100) substrates by HPPMS–PIII&D at a target voltage of 780 V, frequency of 50 Hz, and width of 200 μs in the argon ambient. High-voltage pulses with amplitudes of −8 kV, −12 kV, −16 kV, and −20 kV and the same frequency and pulse width as those of the HPPMS pulses were applied. The V–I characteristics of the HPPMS and PII&D power are showed in Fig. 2. The working pressure was kept at 1.0 Pa and the deposition time is 5 min. Second, N_2 was introduced into the vacuum gradually until the ratio of the Ar to N_2 flow rates was 5 to 3. The CrN thin films were deposited for 60 min using argon and nitrogen. Third, the samples were cooled down in the vacuum chamber at 3×10^{-3} Pa for 30 min. The quality and properties of the CrN/Cr films prepared by HPPMS–PIII&D were compared to those produced by conventional DCMS using the same power.

An AvaSpec-3648 (Netherland) optical emission spectrometer was used to monitor the discharges during conventional DCMS and HPPMS–PIII&D. The structure and thickness of the coatings were determined by scanning electron microscopy (SEM, Hitachi S4800) at 30 kV. The cross-sectional structure and high-resolution lattice images of the interface between the substrate and Cr layer as well as the Cr and CrN layers were investigated by high-resolution transmission electron microscopy (FE-TEM, FEI-TECNAIG2-F30, USA). The changes in the Cr and Fe concentrations at the interface were studied by energy-dispersive X-ray spectroscopy (EDS) equipped on the TEM instrument. The film adhesion was assessed by the scratch method and the morphology was observed on an optical microscope with a magnification of 40X.

3. Results and discussion

A continuous green discharge is observed from the front of the magnetron cathode in the vacuum chamber during HPPMS–PIII&D. The optical emission spectra [21] acquired during the DCMS and HPPMS–PIII&D modes at the same power of 400 W are shown in Fig. 3. In the DCMS discharge, the Ar^{1+} and Cr^0 lines are dominant. A cluster of Ar^0 emission lines between 696.54 nm and 912.30 nm and the Cr^{1+} line at 301.55 nm are also present, but the intensity is smaller. In the HPPMS–PIII&D discharge, emission lines from multiply-charged ions up to a charge stage of three appear, for instance, Ar^{2+} at 272.48 nm, Ar^{3+} at 287.43 nm, Cr^{3+} at 298.82 nm, and Cr^{2+} at 313.32 nm. Cr^{1+} and Ar^{1+} are dominant and the emissions arising from neutrals decrease, suggesting a larger ionized metal flux in HPPMS–PIII&D.

Generally, conventional HPPMS delivers a lower deposition rate than DCMS because a large portion of the ions produced by HPPMS are attracted to the target by the electric field created by the high target voltage [22,23]. However, our experiments indicate that the deposition rate in the hybrid HPPMS–PIII&D technique actually increases significantly, as shown in Fig. 4, which is calculated from the thickness of the films deposited on the Si substrate. Furthermore, the deposition rate goes up as the voltage applied to the sample is increased. A

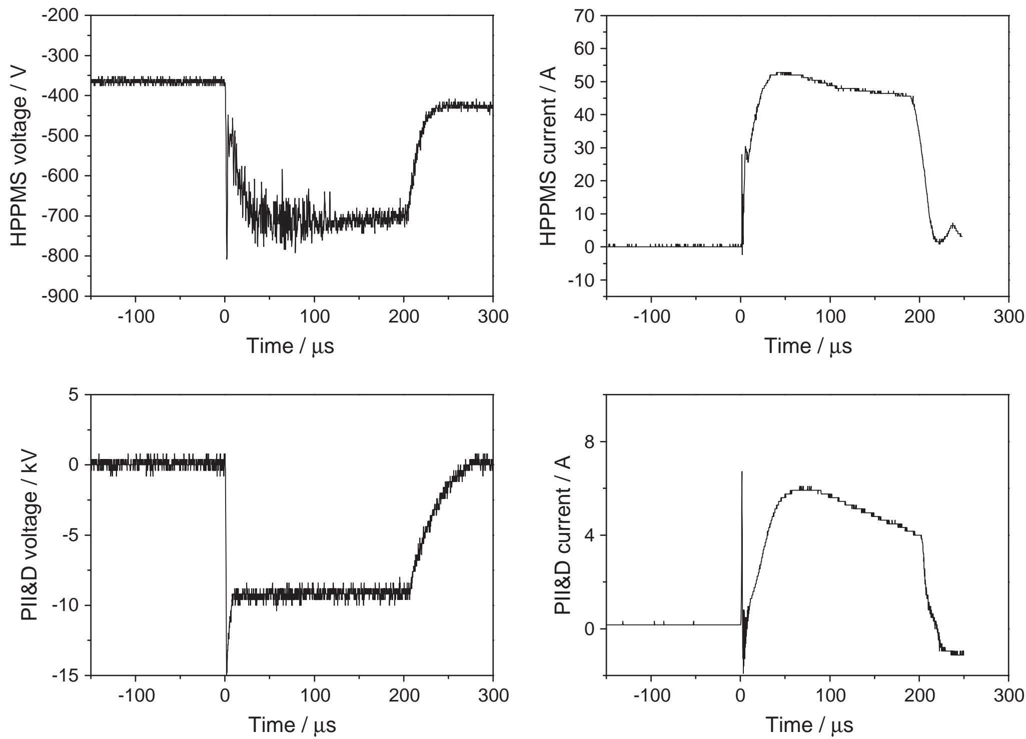

Fig. 2. V–I characteristics of the HPPMS and PII&D power.

maximum rate of 38.3 nm/s is achieved at a high voltage of −20 kV and it is larger than those of conventional HPPMS and DCMS by about 134.7% and 55.4%, respectively. The significant improvement can be attributed to the spatial redistribution of the electric field during HPPMS–PIII&D as more ions are attracted to the sheath created by the sample high voltage.

To experimentally demonstrate the benefits of HPPMS–PIII&D, a CrN/Cr/stainless steel structure is fabricated at a high voltage of −12 kV and the cross-sectional TEM micrograph is depicted in Fig. 5a. Three clearly defined layers correspond to the substrate, a 80 nm Cr interlayer, and a CrN coating with a total thickness of 1 μm. A Cr_xN interfacial layer with a thickness of about 70 nm also appears to be present between the Cr layer and CrN film despite the lack of an apparent interface in the micrograph. The details of the Cr interlayer and top CrN layer are shown in Fig. 5b and c, respectively. The thin layer is composed of many nano-scale equiaxial grains smaller than 10 nm. The grains are quite dense and no voids and pores can be observed. The selected area diffraction pattern acquired from the Cr layer is shown in the inset in Fig. 5b. The distribution and intensity of the diffraction spots suggest that the preferential orientations are Cr (200) and Cr $(11\overline{1})$. The diffraction rings are slightly diffuse implying a nano-scale grain size. The nano-grains are formed as a result of dense nucleation during energetic ion bombardment [24].

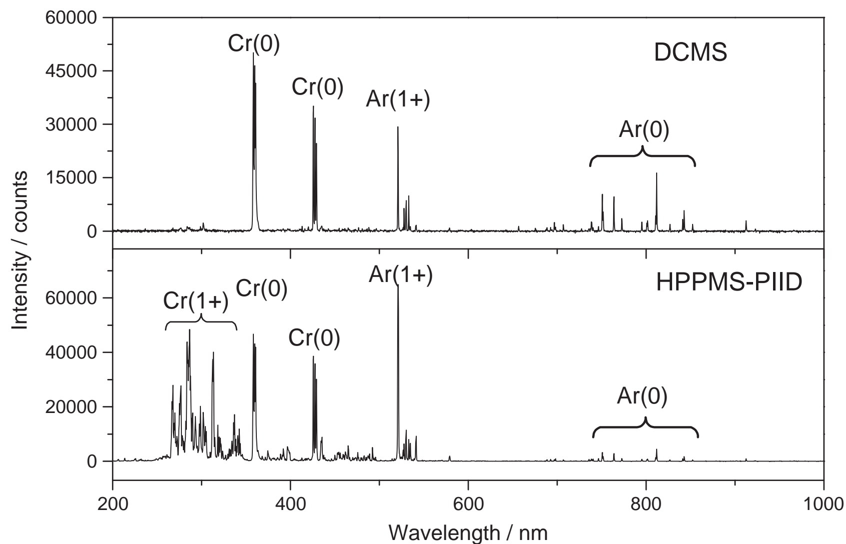

Fig. 3. Optical spectra acquired in DCMS and HPPMS (average power of 400 W).

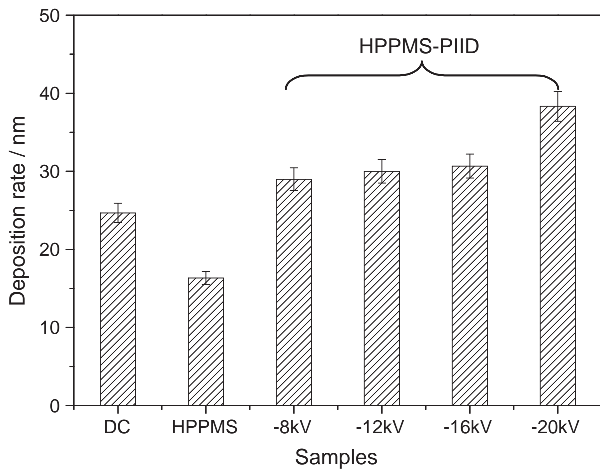

Fig. 4. Comparison of deposition rates in DCMS, HPPMS, and HPPMS–PIII&D (high voltages of −8 kV, −12 kV, −16 kV, and −20 kV and average power of 400 W).

Moreover, the grain size increases gradually from the substrate to CrN layer possibly due to a temperature effect. Equiaxial grains are observed at the interface between the Cr interlayer and CrN layer with a larger grain size. With increasing CrN thickness, the grains morph into a dense columnar microstructure and the grain size increases continuously, indicating high adatom mobility in the initial nucleation stage. Subsequent growth near the interface is competitive and most of the columnar structures are broken resulting in a discontinued morphology. New columns are formed on the existing columns due to a re-nucleation mechanism. The selected area diffraction pattern of the CrN layer is shown in the inset of Fig. 5c. The film has a single phase with the CrN (200) preferential orientation and the Cr to N atomic ratio is 1:1. Our results support the mechanism of a single phase structure as formation of stoichiometric CrN is known to depend on the ion energy during film growth [25,26]. Further TEM observation reveals no macro-particles at the interface or in the coating.

The adhesion characteristics are shown in Fig. 5d. Interfacial layer II between the Cr interlayer and substrate creates strong ionic and covalent bonds [27] compared to the weaker van der Waals forces. It should be noted that there is no obvious boundary between the substrate and Cr interlayer although a band with a thickness of about 40 nm can be observed from the substrate immediately below the interface. Fig. 6 shows the high resolution cross-sectional lattice imaging and compositional changes in interfacial layer II between the stainless steel substrate and the Cr interlayer. As shown in Fig. 6a, no macro-particles or large scale growth defects can be found in the vicinity and the grains in interfacial layer II are extended to the base layer forming a continuous microstructure. The transition between the Cr interlayer and substrate is diffused and defect free. Fig. 6b shows an approximately linear increase in the amount of Fe atoms from the Cr interlayer to the stainless steel substrate while the Cr concentration diminishes gradually. The EDS scan was along the line across the interfacial layer II, as showed in Fig. 5d. The nanostructured layer

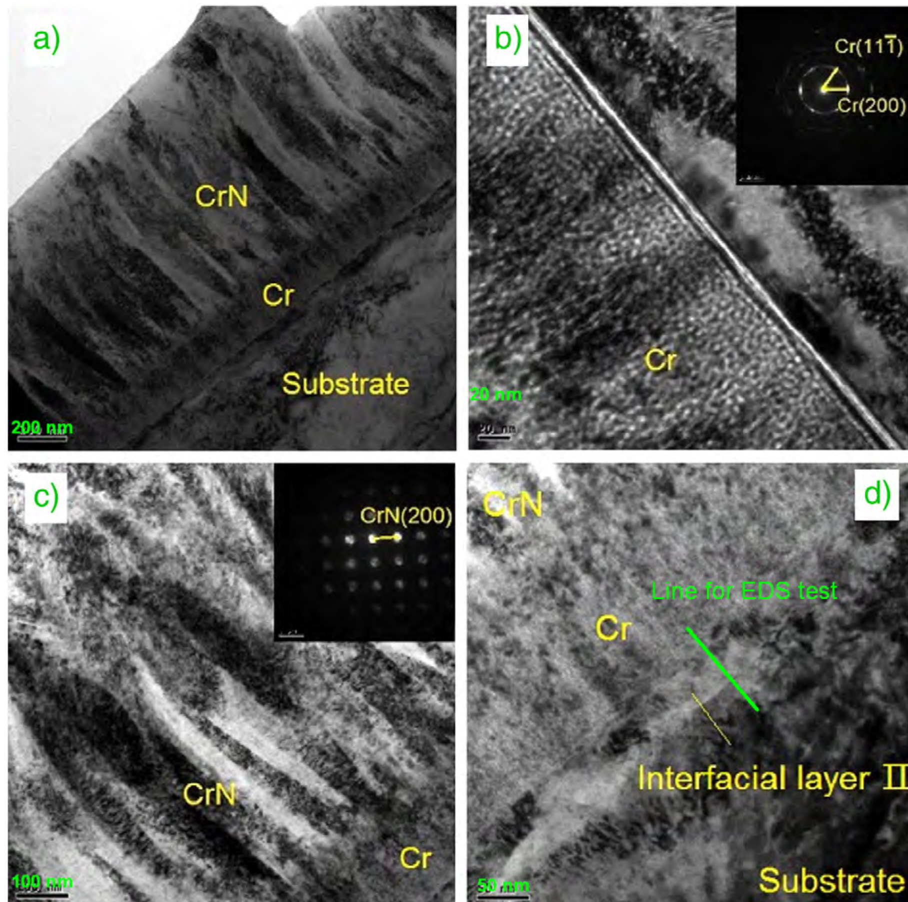

Fig. 5. Cross-sectional TEM micrographs of the sample fabricated by HPPMS–PIII&D using −12 kV: (a) all layers, (b) magnified views of the Cr layer, (c) magnified views of the CrN layer, and (d) magnified view of interfacial layer II. The insets in (b) and (c) are the selected area diffraction patterns obtained from the Cr and CrN layers, respectively.

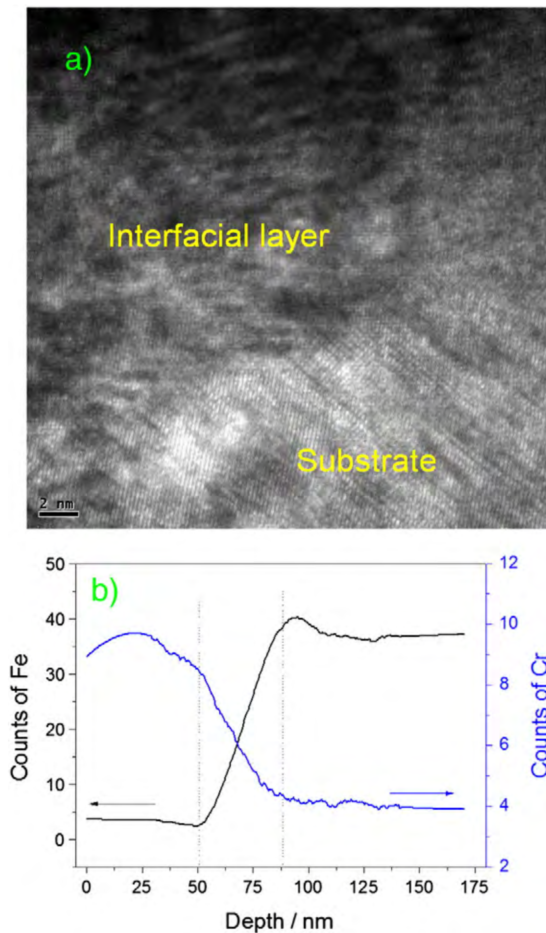

Fig. 6. (a) High-resolution cross-sectional TEM lattice imaging and (b) STEM elemental composition of interfacial layer II obtained from the sample fabricated by HPPMS–PIII&D using a voltage of −12 kV.

between the Cr interlayer layer and substrate has a graded composition which bodes well for film adhesion.

As shown by our data, an interface with weak adhesion force normally formed between the middle layer and substrate is replaced by one with a graded composition and strong adhesion force by the hybrid HPPMS–PIII&D technique. The thickness of the interfacial layer II is 40 nm and can be tailored by control the amplitude of the PII&D voltage, and also, the widths of the HPPMS pulse and PII&D pulse, or the phase difference of the two pulses can be adjusted to realize different ion implantation and deposition modes, such as pure implantation, simultaneous implantation and deposition, or selective implantation [19]. It is in fact about 4 times larger than that prepared by conventional PIII&D at the same sample voltage [28–30]. The CrN bonds strongly to the substrate due to the Cr interlayer and formation of interfacial layers I and II. A critical load of 67.4 N is achieved, compared to 28.8 N for the film produced by DC magnetron sputtering (without interfacial layer II) and 40.8 N for the film prepared using the PCVA source (with a thin interfacial layer II), as shown in Fig. 7. The excellent results suggest that the stress between the ceramic CrN film and stainless steel substrate is reduced significantly by the 40 nm thick interfacial layer II. Successful fabrication of interfacial layer II and the dense and pore free microstructure of the interfacial structure stem from two factors, the highly ionized metallic plasma without metallic droplets produced by HPPMS and high ion energy as a result of the negative voltage applied to the sample during PIII&D. As a result of energetic ion bombardment, significant ion mixing and atomic diffusion occur forming stronger ionic and covalent bonds which increase the adhesion strength.

4. Conclusion

The hybrid HPPMS–PIII&D technique is utilized to produce interfacial structures between the substrate and interlayer as well as interlayer and top coating. Successful fabrication of the interfacial layer between the substrate and interlayer and the dense and pore free microstructure of the interfacial structure can be attributed to the highly ionized metallic plasma without metallic droplets produced by HPPMS and high ion energy as a result of the negative voltage applied to the sample during PIII&D. To demonstrate the benefits of the hybrid technique and fabrication strategy, a CrN/Cr/steel structure is produced by HPPMS–PIII&D and the 40 nm thick interfacial layer formed between the substrate and Cr interlayer releases the interfacial stress. The technique and fabrication strategy have many potential applications, for example, photovoltaics, energy storage, tribological coatings, lubrication, aeronautics, and astronautics.

Acknowledgements

This work was financially supported jointly by Natural Science Foundation of China (No. 51301004), China Postdoctoral Science Foundation (No. 2013M530010), State Key Lab of Advanced Welding and Joining, Harbin Institute of Technology (No. AWJ-M13-13), and City University of Hong Kong Applied Research Grant (ARG) No. 9667066.

References

[1] D. Butler, Nature 454 (2008) 558–559.
[2] J. Chmiola, C. Largeot, P.L. Taberna, P. Simon, Y. Gogotsi, Science 328 (2010) 480–483.
[3] M. Sayer, K. Sreenivas, Science 247 (1990) 1056–1060.
[4] M. Chhowalla, G.A.J. Amaratunga, Nature 407 (2000) 164–167.

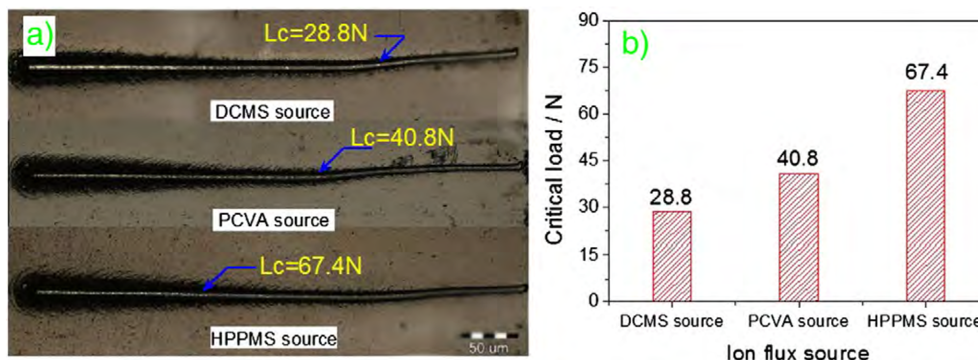

Fig. 7. (a) Morphology of the scratch and (b) critical loads of the samples produced with DCMS, FCVA, and HPPMS.

[5] R.M. Costescu, D.G. Cahill, F.H. Fabreguette, Z.A. Sechrist, S.M. George, Science 303 (2004) 989–990.
[6] J.W. Reiner, F.J. Walker, C.H. Ahn, Science 323 (2009) 1018–1019.
[7] J.A. Floro, E. Chason, R.C. Cammarata, D.J. Srolovitz, MRS Bull. 27 (2002) 19–25.
[8] L. Pocivavsek, R. Dellsy, A. Kern, S. Johnson, B. Lin, K.Y.C. Lee, E. Cerda, Science 320 (2008) 912–916.
[9] R.K. Singh, D.R. Gilbert, J. Fitz-Gerald, S. Harkness, D.G. Lee, Science 272 (1996) 396–398.
[10] Y.S. Li, Y. Tang, Q. Yang, J. Maley, R. Sammynaiken, T. Regier, C. Xiao, A. Hirose, ACS Appl. Mater. Interfaces 2 (2010) 335–338.
[11] J.R. Conrad, J.L. Radtke, J. Appl. Phys. 62 (1987) 4591–4596.
[12] Q. Sun, L. Xia, X. Ma, M. Sun, Appl. Surf. Sci. 206 (2003) 53.
[13] A. Anders, Surf. Coat. Technol. 93 (1997) 158–167.
[14] L. Wang, L. Huang, Z. Xie, X. Wang, B. Tang, Rev. Sci. Instrum. 79 (2008) 023306.
[15] D.M. Sanders, A. Anders, Surf. Coat. Technol. 133–134 (2000) 78–90.
[16] G.S. Bales, R. Bruinsma, E.A. Eklund, R.P. Karunasiri, J. Rudnick, A. Zangwill, Science 249 (1990) 264–268.
[17] V. Kouznetsov, K. Macák, J.M. Schneider, U. Helmersson, I. Petrov, Surf. Coat. Technol. 122 (1999) 290–293.
[18] A.P. Ehiasarian, Y.A. Gonzalvo, T. Whitmore, Plasma Processes Polym. 4 (2007) S309–S313.
[19] Z.Z. Wu, X.B. Tian, J.W. Shi, C.Z. Gong, S.Q. Yang, P.K. Chu, Rev. Sci. Instrum. 69 (2011) 033511.
[20] X.B. Tian, Z.Z. Wu, C.Z. Gong, China Patent, CN, 201010213894.4, 06(2010).
[21] R.W.P. McWhirter, R.G. Huddlestone, S.L. Leonard, New York: Academic Press, **208** (1965).
[22] D.J. Christie, Czech. J. Phys. 56 (2006) B93–B97.
[23] A. Anders, J. Vac. Sci. Technol. A 28 (2010) 783–790.
[24] M. Lattemann, A.P. Ehiasarian, J. Bohlmark, P.Å.O. Persson, U. Helmersson, Surf. Coat. Technol. 200 (2006) 6495–6499.
[25] C. Gautier, H. Moussaoui, F. Elstner, J. Machet, Surf. Coat. Technol. 254 (1996) 86–87.
[26] X.-M. He, N. Baker, B.A. Kehler, K.C. Walter, M. Nastasi, Y. Nakamura, J. Vac. Sci. Technol. A 18 (2000) 30–36.
[27] S.J. Bull, E.G. Berasetegui, Tribol. Int. 39 (2006) 99–114.
[28] A. Anders, Surf. Coat. Technol. 156 (2002) 3–12.
[29] R.M. Oliveira, M. Ueda, B. Moreno, L. Hoshida, S. Oswald, E. Abramof, Phys. Stat. Sol. (c) 5 (2008) 893–896.
[30] C. Reinhard, A.P. Ehiasarian, P.E. Hovsepian, Thin Solid Films 515 (2007) 3685–3692.